RSC Applied Polymers

PAPER

View Article Online
View Journal | View Issue



Cite this: *RSC Appl. Polym.*, 2026, **4**, 626

# Functionalized nanocellulose for efficient removal of ammonium impurities from contaminated water

Priyanka Sharma, *[a] Eyad Mohammed A. Alfarsi,[a] Stanley C. Hicks,[a] Miles Anthony Miller,[a] Saikumar Muddapu,[a] Abbygayle Razalind Ruggiero,[a] William Borges,[b] Julian J. Koebbe,[c] Michael Kahwaji,[c] Anindya K. Swarnakar[d] and James Springstead[a]

Carboxycellulose nanofibers with carboxylate functionality are a promising material for a multitude of applications, including environmental remediation. In this paper, we present an in-depth systematic study on the application of TEMPO-oxidized CNFs for ammonium removal, demonstrating their versatility against a broad range of ammonium impurities (5–5000 ppm) using both simulated and real contaminated water. The efficiency of CNFs was tested under various conditions, including the amount of CNFs, pH, and time. The results showed that CNFs follow both the Langmuir and the Freundlich isotherm models with good fitting, indicating their monolayer as well as multilayer adsorption mechanism. Furthermore, characterization using FTIR, SEM/EDS, and adsorption and kinetic analyses employing various models reveals that chemisorption is the dominant mechanism of ammonium adsorption by CNFs. The Langmuir isotherm model, when fitted to adsorption data gathered for original ammonium impurities in the range of 5–5000 ppm using CNFs, yielded a maximum adsorption capacity of 303.3 mg $g^{-1}$. Additionally, this study includes a technical application to remove ammonium impurities from real contaminated fish water, with results indicating an average removal efficiency of between 80% and 90%. We have also developed an in-house flotation remediation system (FRS) to address handling and collection issues related to CNFs and used CNFs. Hence, this study presents a comprehensive and sustainable approach to addressing the most significant ammonium nutrient problem, utilizing the most abundant, scalable, and eco-friendly plant-based material.

Received 3rd July 2025,
Accepted 15th November 2025

DOI: 10.1039/d5lp00201j

rsc.li/rscapplpolym



## Introduction

Several factors, including the ever-increasing human population, expansive industrial activities, and the subsequent rapid development of industries, have been attributed to an increase in the use of anthropogenic ammonia ($NH_3$) and an increase in ammonium ion ($NH_4^+$) deposition in aquatic environments. A considerable amount of $NH_4^+$ in the aquatic environment originates from human excreta, which contains nitrogenous compounds metabolized by bacteria into $NH_4^+$. Additionally, agricultural runoff, particularly from areas with extensive use of nitrogen-based fertilizers, significantly contributes to $NH_4^+$ pollution.[1] Fertilizers rich in $NH_4^+$ and nitrates are applied to crops to enhance growth; however, their significant amounts leach into surface and groundwater, resulting in elevated $NH_4^+$ levels in rivers, lakes, and aquifers. Globally, Harmful Algal Blooms (HABs) pose a significant environmental challenge, particularly in nutrient-rich water bodies. These blooms, often caused by cyanobacteria (also known as blue-green algae), thrive in warm, slow-moving waters with high levels of phosphorus and nitrogen.[2–4] Excess nutrients, primarily from agricultural runoff, lawn fertilizers, faulty septic systems, and wastewater treatment plants, exacerbate this issue.[5] Phosphorus is the primary driver, as it promotes rapid algal growth, while $NH_4^+$ acts as an additional nutrient source, sustaining these blooms. HABs disrupt aquatic ecosystems by blocking sunlight, depleting oxygen levels during decomposition, and releasing toxins harmful to humans, animals, and marine life. Despite implementing Total Maximum Daily Loads (TMDLs) to regulate phosphorus inputs, toxic HABs remain a recurring issue. Continued efforts to reduce nutrient pollution, restore natural shorelines, and promote public education are crucial to safeguarding freshwater ecosystems.[6,7]

[a]*Department of Chemical and Paper Engineering, Western Michigan University, Kalamazoo, Michigan 49008, USA. E-mail: priyanka.sharma@wmich.edu; Tel: +1-6315423506*
[b]*Yale University, New Haven, CT 06520, USA*
[c]*Richmond Institute of Design and Innovation at Western Michigan University, Kalamazoo, Michigan 49008, USA*
[d]*Department of Chemistry, University of Alberta, Alberta, Canada T6G 2G2*

In industrial settings, $NH_4^+$ concentrations in wastewater can vary significantly, with levels often exceeding regulatory limits. For instance, municipal wastewater has $NH_4^+$ concentrations ranging from 27 to 100 mg $L^{-1}$. Fish-processing waste has $NH_4^+$ concentrations ranging between 8 and 42 mg $L^{-1}$. In domestic wastewater, the $NH_4^+$ concentration typically ranges from 39 to 60 mg $L^{-1}$.[8] Fertilizer production, food processing facilities, and similar industries frequently have $NH_4^+$ concentrations ranging from 5 to 1000 mg $L^{-1}$.[8,9] These values increase depending on the type of processing industry, typically reaching as high as 2945 mg $L^{-1}$. $NH_4^+$ plays a crucial role in both aquatic and terrestrial environments, particularly within the nitrogen cycle.[8] It can exist in equilibrium with ammonia ($NH_3$) in aqueous solutions, and the equilibrium between $NH_4^+$ and $NH_3$ is highly dependent on pH. At lower pH levels, $NH_4^+$ is predominant, while at higher pH levels, $NH_3$ dominates.[10] $NH_4^+$ in drinking water poses significant health risks. For example, it can react with chlorine during water treatment processes to form chloramines, which can exacerbate asthma symptoms due to excessive exposure to trichloramine.[11] Additionally, when $NH_4^+$ is oxidized to nitrite in the human body, it can interfere with the oxygen-carrying capacity of hemoglobin, particularly in infants, leading to methemoglobinemia, commonly known as "blue baby syndrome".[12] Therefore, there is an urgent need to address $NH_4^+$ in wastewater in a sustainable manner.

It can be removed through various methods, including biological treatment, adsorption techniques,[13,14] and chemical precipitation. Adsorption is the most promising technique investigated for removing $NH_4^+$ from wastewater. Unfortunately, this technique is often marred by a lack of suitable and viable adsorbent materials. According to Han *et al.*,[15] this challenge is further aggravated by the need to find efficient, affordable, abundant, and sustainable materials. Consequently, different avenues have been explored, including modifying adsorption techniques to accommodate various materials. Wang *et al.*[16] reported that physical activation and chemical modification are the most prominent avenues for enhancing the performance of ion exchange mechanisms based on readily available adsorbent materials. For instance, the authors sought to examine whether physical activation could enhance the adsorption method for removing $NH_4^+$ using forestry waste.[17,18] Several recent studies have focused on the adsorption of ammonium using activated carbon (AC).[18] In addition to this, a few more carbon adsorbents, such as cellulose acetate membrane, AC derived from bacterial cellulose,[18] and cellulose sulfate,[19] have been used to address the $NH_4^+$ problem. To the best of our knowledge, none of the studies have in-depth discussed the use of carboxylated cellulose nanofibers (CNFs) for the remediation of $NH_4^+$ pollutants from real and simulated water, and have not provided a practical solution to tackle this problem sustainably. In this study, we have done a systematic in-depth study to apply the CNFs to remediate the $NH_4^+$ pollutant from the simulated and real water (from the aquaponic tank), followed by the development of a floatation remediation system (FRS) to ease the handling and to provide the viability of the CNFs adsorbent system for all types of contaminated water sources.

## Experimental section

### Materials and instruments

TEMPO-oxidized cellulose nanofibers extracted from the forest biomass with a concentration of 1.04 wt% and a carboxylate ($COO^-$) content of 1.15 mmol $g^{-1}$ were procured from the University of Maine. Analytical ammonium nitrate (ACS reagent, 99%) and sodium bicarbonate (ACS reagent, ≥99.7%) were purchased from Sigma-Aldrich. Sodium hydroxide (ACS reagent, ≥97.0%) pellets and hydrochloric acid (ACS grade, 36.5–38%) were purchased from Fisher Scientific. An ammonium ion-selective electrode was used to measure the concentration of $NH_4^+$. The following instruments were used in this study.

Fourier transform infrared spectrometry (FTIR): A ThermoFisher instrument (ThermoFisher Scientific, U.S.A.) was used to record the FTIR spectra in transmission mode, between 4000 to 450 $cm^{-1}$. A total of 12 scans were taken per sample with a resolution of 4 $cm^{-1}$. The solid samples were recorded in attenuated total reflectance (ATR) mode.

The JEOL 7500F ultra-high-resolution scanning electron microscope, equipped with a cold-field emission emitter, was used to examine the morphology of CNFs. Zeta potential measurements on CNFs samples were performed using MÜtek™ PCD-06, Particle Charge Detector.

### Preparation of ammonium solutions

A 5000 ppm $NH_4^+$ stock solution was prepared by dissolving 22.22 g of $NH_4NO_3$ in 1 L of deionized water. Serial dilutions were made to range from 5000 to 5 ppm for use in adsorption studies.

### Preparation of cellulose nanofibers (CNFs) suspension

CNFs suspension was prepared using commercial TEMPO-oxidized CNFs gel at an initial concentration of 1.04% (wt%) with carboxylate ($COO^-$) content of 1.15 mmol $g^{-1}$. The CNFs were diluted to 0.5% (wt%) by adding deionized water under continuous stirring. The suspension was homogenized to ensure an even distribution of the nanofibers. This CNF's suspension was used as an adsorbent for the $NH_4^+$ adsorption experiments.

### Remediation studies using simulated water

The concentration of active $NH_4^+$ in the solution was determined using an ion-selective electrode. For the adsorption capacity experiments, 5 mL of CNFs suspension was mixed with 5 mL of $NH_4^+$ solution (prepared from ammonium nitrate) in a test tube. In this study, $NH_4^+$ concentration is reported as parts per million (ppm) of $NH_4^+$ to maintain consistency with other studies that may employ different $NH_4^+$ salts. However, the specific $NH_4^+$ salt used is noted to account for any potential counter-ion effects.

For all experiments except the time study, the solution was stirred for 1 minute and then incubated at room temperature for 24 hours. After incubation, the samples were filtered using a syringe filter with a 0.22 μm pore size, showing effective separation. The filtrate was then analyzed for $NH_4^+$ concentration using an ion-selective electrode. To ensure that the syringe material did not contribute to $NH_4^+$ adsorption during the experiment, a control test was conducted. A solution of $NH_4^+$ with an initial concentration of 500 ppm was prepared and passed through the syringe without any additional materials or treatments inside. The difference in concentration was negligible, confirming that the syringe material did not significantly interfere with the adsorption of $NH_4^+$.

### pH study

To study the effect of pH on adsorption capacity, the pH of the $NH_4^+$ was adjusted to the desired levels using dilute sodium hydroxide or hydrochloric acid. After pH adjustment, the solutions were mixed with a 0.5% CNFs suspension at a 1 : 1 ratio. The mixtures were then incubated at room temperature for 24 hours.

### Time study

Additionally, a study assessed the adsorption capacity over different incubation times ranging from 0.5 to 48 hours using an initial $NH_4^+$ concentration of 500 ppm. The $NH_4^+$ concentration in the filtrate was measured at each time point to evaluate the effect of contact time on adsorption efficiency.

### Remediation studies using real water

The contaminated water was collected from the real fish tank located in the Greenhouse Facility at Western Michigan University's Department of Biology. The water was collected directly from the tank before it passed through the *in situ* filtration. The $NH_4^+$ concentration before and after adsorption using a CNFs suspension was determined using an $NH_4^+$ test kit, followed by quantitative measurement using UV-adsorption. The details are mentioned in the SI.

### Floc separation procedure

The floc term refers to the gel material that forms when CNFs interact with $NH_4^+$ impurities, causing the suspended CNF fibers to clump together into a lumpy gel. The separation of the floc was performed in the following steps. A 5 mL suspension of 0.5 wt% CNFs having $COO^-$ groups was mixed with 5 mL of $NH_4^+$ solution prepared from $NH_4NO_3$ for simulated water testing at different concentrations from 5000 to 5 ppm (SI) in a test tube. In contrast, the water collected from the fish tank contained its own $NH_4^+$ impurities (SI). The solution was gently shaken for 1 minute and then incubated at room temperature for 24 hours to neutralize the charges and initiate the aggregation of CNFs and adsorbed $NH_4^+$ into flocs. For separation, the flocs were filtered through a vacuum filtration system equipped with a 0.45 μm membrane filter (Fig. 1). The retained flocs on the membrane were oven-dried and analyzed for further characterization.

## Results and discussion

### Chemical and morphological properties

The FTIR analysis (Fig. 2A), conducted at the dry stage, reveals significant changes in the functional groups of CNFs after exposure to $NH_4^+$, confirming ion exchange as the dominant interaction mechanism. The broad O–H stretching peak around 3338 $cm^{-1}$ in CNFs exhibits slight shifts and intensity reductions, which can be attributed to overall hydrogen bonding alteration due to the interaction of $NH_4^+$ ions. A notable decrease in the intensity of the ($-COO^-$) stretching peak near 1599 $cm^{-1}$ in CNFs suggests the involvement of $-COO^-$ groups in the binding with $NH_4^+$ ions. Additionally, in the floc sample containing CNFs + $NH_4^+$, the emergence or intensification of a peak around 1578 $cm^{-1}$ in the N–H bending vibration provides direct evidence of $NH_4^+$ binding to the CNFs. The C–O stretching peak at approximately 1176 $cm^{-1}$ in CNFs also shows changes in intensity and position, indicative of interactions between $NH_4^+$ and ester or carboxyl groups on the CNFs structure. These spectral changes collectively validate that $NH_4^+$ ions are adsorbed onto CNFs through an ionic interaction process between the carboxylate and ammonium groups (Fig. 2B), followed by changes in the hydrogen bonding in CNFs as evident by the changes in the O–H stretching vibration at 3338 $cm^{-1}$.[20] The observations emphasize the crucial role of the carboxyl and hydroxyl groups in facilitating effective $NH_4^+$ adsorption, making CNFs a promising material for wastewater remediation.[21–28] FTIR analysis

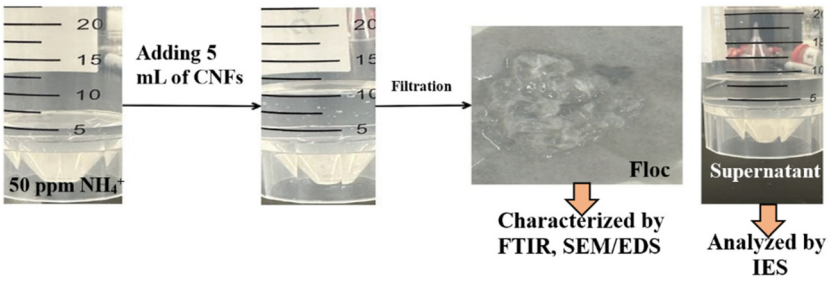


Fig. 1 Demonstration of floc preparation and separation of supernatant from the floc for further characterization.

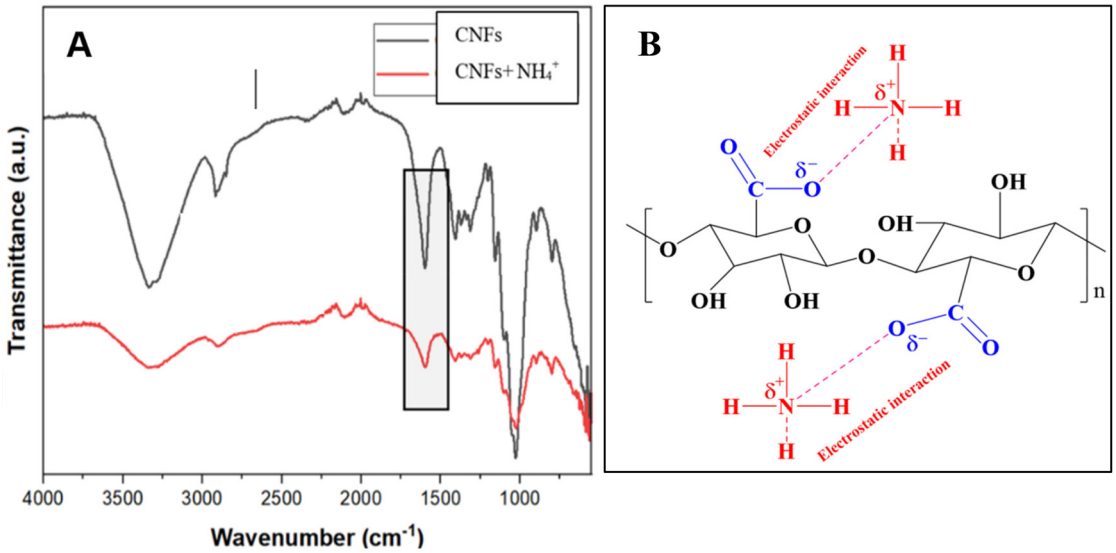


Fig. 2 (A) FTIR of CNFs and floc (CNFs and $NH_4^+$), (B) schematic of the mechanism of CNFs and $NH_4^+$ interaction.

(Fig. 3) was further supported by the morphological changes that occurred before and after the $NH_4^+$ interactions on CNFs.

The morphological analysis conducted *via* SEM/EDS reveals significant structural changes in CNFs as the concentration of $NH_4^+$ varies. One hundred fibers were selected from each image, and their dimensions were measured using ImageJ software to ensure statistical reliability. Pristine CNFs (Fig. 3A and Fig. S1 in SI) exhibited a maximum fiber diameter between 15.4 and 18.1 nm. However, after exposure to 5 ppm $NH_4^+$ (Fig. 3B and Fig. S1 in SI), the range increased to 19.7–22.8 nm, indicating swelling of the individual fibers. Notably, when the CNFs were further exposed to a higher concentration of 5000 ppm $NH_4^+$ (Fig. 3C and Fig. S1 in SI), the range increased to 21.3 and 24.8 nm, demonstrating substantial structural changes due to the intake of $NH_4^+$. The swelling of individual cellulose fibers illustrates the mechanism of $NH_4^+$ removal, which can be explained by (i) an ion-exchange mechanism: the size of the $NH_4^+$ ion is 140 pm, which is

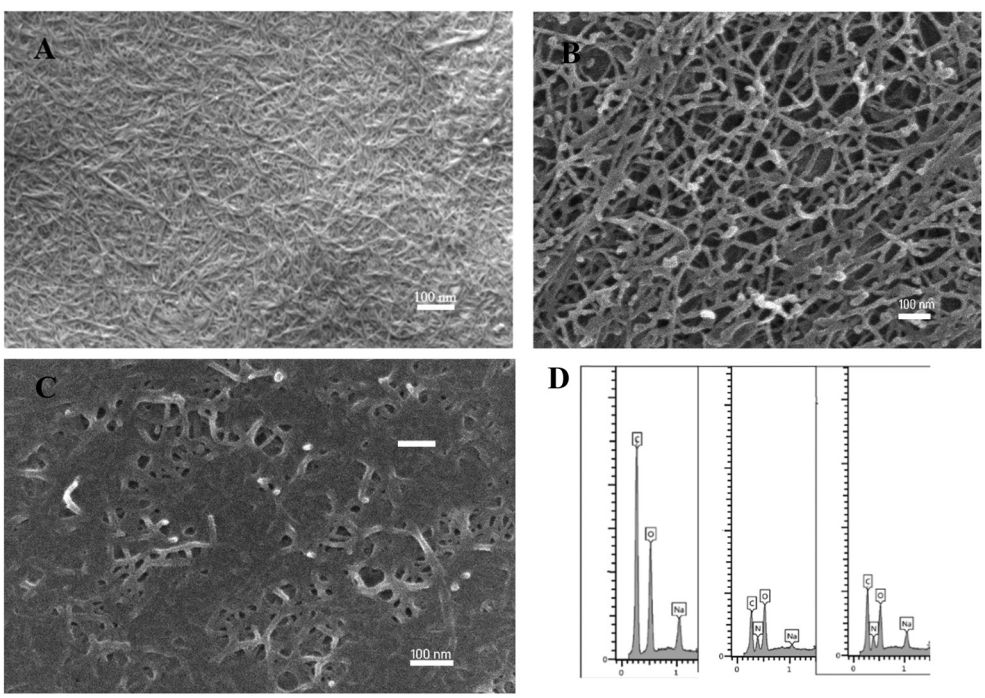


Fig. 3 SEM images of CNFs at different $NH_4^+$ concentrations, (A) CNFs; (B) CNFs + $NH_4^+$ (5 ppm); (C) CNFs + $NH_4^+$ (5000 ppm); (D) A, B, C respective EDS spectra.

larger than that of Na (95 pm) or H (0.208 nm). The $Na^+$ or $H^+$ is associated with the carboxyl ($-COO^-$) groups on the CNFs. During the interaction of CNFs and $NH_4^+$ ions for remediation, the increase in fiber diameter indicates the $NH_4^+$ ions replacement with the CNF's carboxyl counterions. These results are consistent with the FTIR results, further supporting ion exchange and indicating ionic interactions. This ion exchange corresponds to the absorption phenomenon. Hence, different isotherm models, as presented in the adsorption studies section, are used to analyze the adsorption efficiency of CNF fibers. (ii) Absorption: Typically, the CNF's fiber width is between 4 and 6 nm. Here, the CNFs we have used have a maximum diameter between 15.4 and 18.1 nm, indicating that CNFs still retain a layered structure, which may have led to the absorption of impurities on the CNFs. The EDS analysis (Fig. 3D) depicts significant changes in the elemental composition of CNFs before and after $NH_4^+$ adsorption. Initially, the pristine CNFs sample (Fig. 3D) contains 7.9 wt% of sodium (Na), with no detectable nitrogen (N) present. After exposure to 5 ppm $NH_4^+$ (Fig. 3D), the wt% of Na decreases to 3.4 wt%, while nitrogen appears at 21.9 wt%, indicating the successful adsorption of $NH_4^+$ ions onto the CNF's surface. This trend changes at 5000 ppm $NH_4^+$ (Fig. 3D), where Na increases to 10.1 wt%, and nitrogen decreases to 17.7 wt%. This indicates that at a higher concentration of $NH_4^+$, absorption is more dominant than ion exchange. To confirm these results further, elemental analysis is recommended. The indication of nitrogen in the elemental composition strongly supports the intake of $NH_4^+$, highlighting CNF's effectiveness as an adsorbent for $NH_4^+$ removal in wastewater treatment. We have also performed zeta potential measurements to investigate the change in surface charges of CNFs upon interaction with different $NH_4^+$ impurities. The results indicate that the surface charge of CNFs at a concentration of 0.0125 w% showed a charge of $-418.5\ \mu g\ L^{-1}$. When 5 ppm $NH_4^+$ was added, the charge decreased to $-283.8\ \mu g\ L^{-1}$, and further addition of 250 ppm $NH_4^+$ reduced the surface charge to $-222.6\ \mu g\ L^{-1}$. This trend of decreasing the surface charge of CNFs with an increase in ammonium concentration further evidences the presence of ionic interactions between these two functionalities.

## Adsorption studies

**pH study.** In this study, the removal of $NH_4^+$ was significantly influenced by the solution's pH (Fig. 4A and Table S1 in SI), which affects the equilibrium between $NH_4^+$ and $NH_3$. At lower pH values, $NH_4^+$ is the dominant species, which facilitates electrostatic attraction between the positively charged $NH_4^+$ and the negatively charged surface ($COO^-$) of CNFs, leading to higher adsorption efficiency. However, at pH 3, the removal efficiency was only 7%, despite $NH_4^+$ being the predominant species. This low removal efficiency can be attributed to the fact that at pH 3, the solution contains a high concentration of free $H^+$ ions. These $H^+$ ions compete with $NH_4^+$ for the active adsorption sites on the adsorbent surface. Since $H^+$ ions are more abundant, they preferentially occupy the available sites, further reducing the ability of $NH_4^+$ to be adsorbed. As a result, both electrostatic repulsion and competition for adsorption sites contribute to the low removal efficiency of $NH_4^+$ at this pH level.

As the pH increased from 3 to 7, the removal efficiency increased, reaching a peak of 98% at pH 7, corresponding to the highest concentration of $NH_4^+$ and a favorable interaction between the adsorbent surface and the $NH_4^+$. Beyond pH 7, the removal efficiency plateaued at around 85% and slightly decreased due to the deprotonation of $NH_4^+$ to $NH_3$, which is neutral and, therefore, less effectively adsorbed onto the adsorbent surface. Additionally, the adsorbent surface began to turn non-ionic (COONa), which decreased the number of $COO^-$ groups available for interaction with $NH_4^+$, further reducing the removal efficiency. However, at pH 9, it still maintained a removal efficiency of 85%.

**Effect of adsorbate dose.** The influence of CNFs dosage on $NH_4^+$ removal efficiency (Fig. 4B and Table S2 in SI) reveals a notable trend: as the CNFs weight percentage increases, the

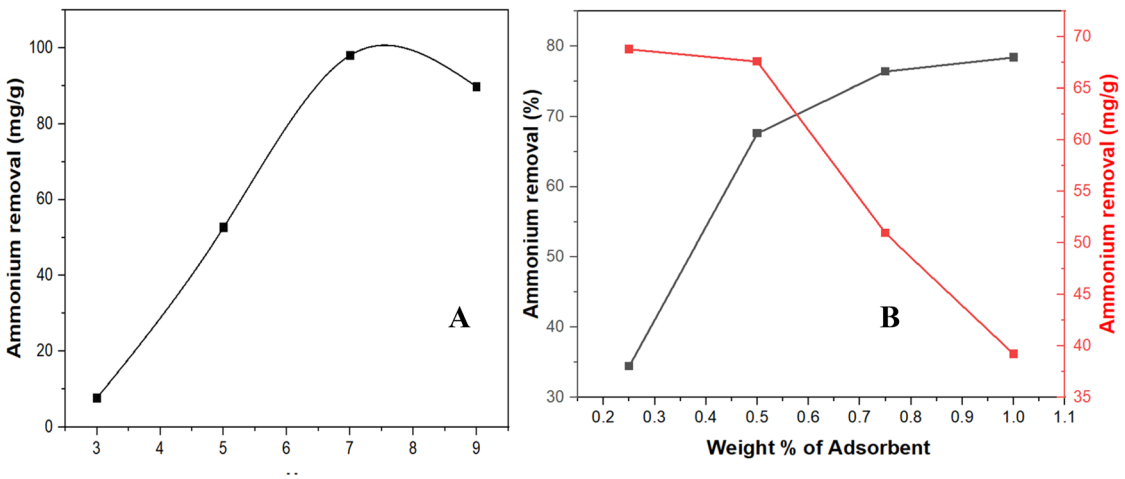


Fig. 4 (A) Effect of initial pH on the removal efficiency of $NH_4^+$; (B) effect of adsorbent dose on $NH_4^+$ removal.

removal efficiency significantly improves, peaking at approximately 78.4% with a 1% CNFs dosage. Notably, no pH adjustment was done for this experiment. This enhancement is attributed to the rise in active adsorption sites that accompany a higher amount of CNFs, facilitating a more effective capture and removal of $NH_4^+$ from the solution. An increased CNFs dosage results in a larger surface area, providing more binding opportunities for $NH_4^+$ and enhancing adsorption and absorption performance. However, it is essential to note that while the removal efficiency increases with higher CNFs dosages, the equilibrium adsorption capacity ($Q_e$) exhibits a decreasing trend (Fig. 5A). The calculations for $Q_e$ and equilibrium concentration ($C_e$) are presented in SI, Table S3. For instance, at a 0.25% CNFs concentration, the removal efficiency is only 34.4%, but the $Q_e$ is relatively high at 67.6 mg $g^{-1}$ (Table S2, SI). As the CNF dosage increases to 1.0%, the removal efficiency rises to 78.4% while $Q_e$ decreases. This behavior occurs because, with higher CNF dosage, there are more active adsorption sites than $NH_4^+$ in the solution, resulting in underutilization of the available sites. Consequently, the amount of $NH_4^+$ adsorbed per unit weight of CNFs ($Q_e$) decreases despite the overall improvement in removal efficiency.

It is also important to emphasize that the increase in removal efficiency begins to stabilize at higher CNF concentrations, as outlined in Fig. 4B and Table S2 of the SI. This indicates that, beyond a certain point, the efficiency is not simply limited by the number of available active sites. Instead, factors such as site saturation, diffusion limitations, and potential agglomeration of CNFs at elevated concentrations can influence effectiveness by reducing the available surface area for interaction. Therefore, after the 1.0% dosage, further increases in CNFs are unlikely to yield significant improvements in removal efficiency, underscoring the importance of optimizing the dosage to achieve excellent results.

**Equilibrium adsorption capacity ($Q_e$) of CNFs.** The effect of $NH_4^+$ concentration on the adsorption capacity of CNFs reveals a significant and compelling trend, as shown in Fig. 5A. As the initial concentration of $NH_4^+$ increases, the $Q_e$ of CNFs shows a substantial rise. At lower concentrations, specifically within the 0 to 1000 mg $L^{-1}$ range, $Q_e$ experiences a sharp ascent, reaching approximately 120 mg $g^{-1}$. This notable increase suggests that many active sites on the CNF's surface are readily available for efficient adsorption. As the concentration increases from 1000 to 5000 mg $L^{-1}$, $Q_e$ rises at a slower and more gradual pace, ultimately achieving a value of around 250 mg $g^{-1}$. This trend indicates that the active sites on the CNFs are progressively approaching saturation. The line on the graph in Fig. 5A represents a predicted trend that is relatively close to the experimental data, confirming the reliability of the results. This agreement not only reflects the reliability of the adsorption effect but also demonstrates the effectiveness and versatility of CNFs as an adsorbent agent. This alignment highlights the reliable nature of the adsorption behavior and underscores the exceptional performance and diverse abilities of CNFs as an effective adsorbent material. These findings demonstrate that CNFs are a highly effective medium for capturing $NH_4^+$ across a range of concentrations. Its impressive adsorption capacity diminishes only as the active sites near full occupancy. This behavior is characteristic of adsorption processes, where an initial solid driving force, resulting from electrostatic interactions, facilitates rapid molecular uptake *via* ion-exchange, which gradually slows as equilibrium is reached. Utilizing CNFs as an adsorbent presents a strategic and effective solution for efficiently removing $NH_4^+$.

**Adsorption isotherm.** The adsorption behavior of $NH_4^+$ onto CNFs was investigated at various concentrations and analyzed using Langmuir and Freundlich isotherm models (Fig. 5A, B, Table 1, and Tables S3, S4 in SI). The Langmuir model revealed a maximum adsorption capacity ($Q_m$) of 303.03 mg $g^{-1}$, accompanied by a Langmuir constant ($K_L$) of 0.0033 L $mg^{-1}$, indicating a highly efficient monolayer adsorption process.[29] In contrast, the Freundlich model displayed a heterogeneity index ($n$) of 0.8211, suggesting a particularly favorable adsorption process on a heterogeneous surface, especially at lower

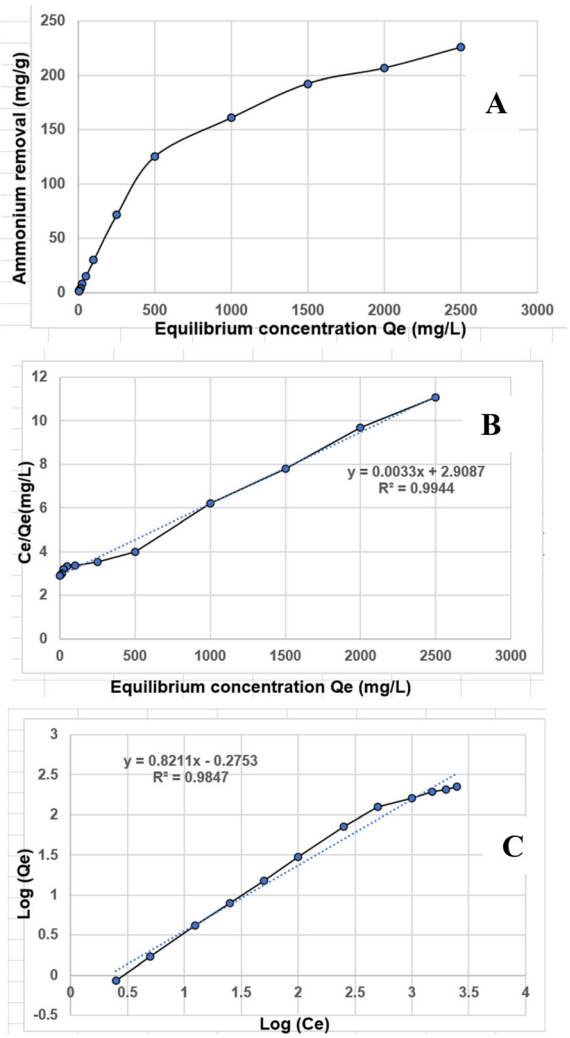


Fig. 5 (A) Relationship between $NH_4^+$ removal and equilibrium concentration; (B) Langmuir isotherm for $NH_4^+$ removal using CNFs; (C) Freundlich isotherm for $NH_4^+$ removal using CNFs.

**Table 1** Isotherm model parameters for $NH_4^+$ adsorption using CNFs

| Isotherm model | Parameter | Value |
|---|---|---|
| Langmuir model | Maximum adsorption capacity ($Q_{max}$) | 303.03 mg $g^{-1}$ |
| | Langmuir constant ($K_L$) | 0.0033 L $mg^{-1}$ |
| | $R^2$ | 0.9944 |
| Freundlich model | Freundlich constant ($K_F$) | 0.302 mg $g^{-1}$ (L $mg^{-1}$) 1/$n$ |
| | Heterogeneity index ($n$) | 0.8206 |
| | $R^2$ | 0.9847 |

$NH_4^+$ concentrations. The high $R^2$ values of 0.9944 for the Langmuir model and 0.9847 for the Freundlich model demonstrate an excellent fit for both models, emphasizing the involvement of adsorption (ion-exchange) and absorption (due to multilayered CNFs) in the removal of $NH_4^+$ using CNFs. The adsorption efficiency values in Tables S3 and S4 of the SI provide further insight into this mechanism. This suggests that at concentrations of 250 ppm and above, adsorption may be predominantly dominated by monolayer interactions due to the high concentration of impurities. In contrast, at lower concentrations (5–500 ppm), multilayered absorption is a more pronounced mechanism, probably due to increased diffusion facilitated by lowered concentration of $NH_4^+$ impurities, reflecting the complex and adaptive surface chemistry of CNFs. The linearized Langmuir plot $C_e/Q_e$ *vs.* $C_e$ (Fig. 5B) showed a clear linear trend with an $R^2$ value of 0.9944, confirming the reliability of the Langmuir model in describing the adsorption behavior. On the other hand, the Freundlich model (Fig. 5C) offered valuable insights into adsorption at lower concentrations. It provided a heterogeneity index ($n$) of 0.8211 and a Freundlich constant ($K_F$) of 0.302 (L $mg^{-1}$)^(−1/$n$), emphasizing the varied nature of the CNFs' surface. The Freundlich plot ($\log(Q_e)$ *vs.* $\log(C_e)$) also showed a strong fit with the experimental data, with an $R^2$ value of 0.9847. This model reflects the heterogeneous nature of the CNF's surface, where adsorption occurs at sites with varying affinities for $NH_4^+$ ions. The slope (1/$n$) suggests that the adsorption process is particularly favorable (with a nice fit) at lower $NH_4^+$ concentrations, where multilayer adsorption and diverse interactions become significant. These results highlight the dual nature of $NH_4^+$ adsorption onto CNFs. These findings confirm the potential of CNFs as a robust and adaptable material for wastewater treatment and environmental remediation, capable of effectively responding to changing conditions and ion concentrations.

**Adsorption kinetics.** The adsorption kinetics of $NH_4^+$ removal using CNFs were evaluated using the $Q_t$ *vs.* $T$ and $T/Q_t$ *vs.* $T$ plots. The $Q_t$ *versus* $T$ plot (Fig. 6A and Tables S5 and S6 in the SI) shows that the adsorption capacity ($Q_t$) increases from 65 mg $g^{-1}$ to ~85 mg $g^{-1}$ within the first 24 hours. This rapid increase can be attributed to the high availability of active binding sites on CNFs at the initial stage, resulting in an efficient uptake of $NH_4^+$. The peak, which occurs around 24 hours, marks a significant point, as the adsorption capacity begins to decline, dropping to approximately 60 mg $g^{-1}$ by 48 hours. This reduction suggests potential desorption due to competitive inhibition among $NH_4^+$. Notably, this peak marks the point at which the adsorption capacity reaches its maximum and begins to decline, indicating the saturation of active binding sites on CNFs. This may also be attributed to possible structural changes in CNFs or the re-equilibration of adsorbed ions back into the solution.

The $T/Q_t$ *versus* $T$ plot (Fig. 6B) was used to further assess the adsorption kinetics, fitting the pseudo-second-order model, which generally indicates chemisorption involving valence forces or covalent bonding. The high $R^2$ value of 0.9827 means that the adsorption process is well-described by this model. This suggests that the adsorption of $NH_4^+$ is rate-limited by the availability of active adsorption sites, following the pseudo-second-order kinetics.[30] The linear fit equation suggests a constant rate of 0.0163 g $mg^{-1}$ hour, confirming the steady rate of the adsorption process. These findings align with previous studies, which indicate that nanocellulose materials, particularly CNFs, provide efficient active sites for $NH_4^+$ adsorption and can be described well using pseudo-second-order kinetics.[31] The kinetic analysis confirms that CNFs hold significant promise for removing $NH_4^+$ from wastewater, with the initial stages of the adsorption process being

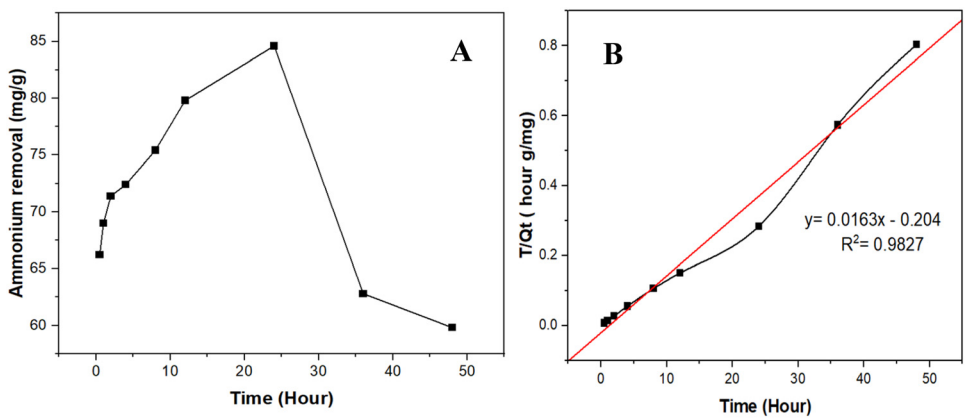


**Fig. 6** (A) Removal of $NH_4^+$ over time using CNFs; (B) Pseudo-second-order kinetics for $NH_4^+$ adsorption by CNFs.

particularly crucial. The potential of CNFs for wastewater treatment is a hopeful sign for the future of environmental science, although optimizing contact time is critical to maintaining high efficiency.

**Comparative study.** As mentioned earlier, biochar is a promising material to remove a wide range of impurities, including $NH_4^+$. Hence, intensive practices have been deployed to increase their efficiency, as shown in Table 2. For example, Zhang *et al.*[33] have used sulfonation to enhance performance. Consequently, the study investigated the capacity of giant reed stalks to strengthen the production of biochar. Study results from Langmuir models determined that the combination of sulfonation and giant reed stalks improved the adsorption efficiency of biochar for $NH_4^+$ to 4.20–5.19 mg N $g^{-1}$. Liu and Zhang[35] improved their biochar by combining straw powder and soda residue in the co-pyrolysis process. Their findings indicated that industrial soda residue played a crucial role in enhancing the performance of biochar. In a separate study, Qin *et al.*[32] investigated the effectiveness of biochar enhancement using bamboo in the ball milling process. The outcomes of batch adsorption models revealed the cost-efficiency and impeccable performance of the ball-milled bamboo biochar (BMBB) with $Q_m$ of 29.9 mg $g^{-1}$. Khamkeaw *et al.*[18] found that biochar obtained from bacterial cellulose exhibited an increased adsorption rate, with a maximum removal of ammonium ions at 30 °C ranging from 33.5 to 221.4 mg $g^{-1}$. Other vital materials, such as ion-exchange resin, have also been deployed to tackle the $NH_4^+$ impurities, for example. MIEX resin and pyridinium-type anion exchange resin have shown removal rates of 98% and 94%, respectively. A report showed the use of cellulose sulfate nanofibers with a maximum removal efficiency of 41.1 mg $g^{-1}$. Among these reported carbon materials, the CNFs presented in this study showed the maximum removal of 303.3 mg $g^{-1}$, due to their multilayer structure and surface chemistry, which fit both multilayer and monolayer adsorption models. This is a crucial study that opens up opportunities for applying various types of cellulose fibers to remediate global nutrient pollution.

**Demonstration of the technical application of CNFs in a fish tank.** The CNFs, like material, appeared in a suspension at a concentration of 0.5 wt%. Based on this study, CNFs can exhibit a maximum removal efficiency ($Q_m$) of 303.3 mg $g^{-1}$; however, a significant challenge to adopting this material for technical applications is the handling, transportation, and recovery from the waste site. Hence, to overcome this problem, in collaboration with our Department of Fine Arts and Design at Western Michigan University, we have developed a flotation remediation system (FRS) as shown in Fig. 7, comprised of following parts: (i) dialysis tube to hold the adsorbent, more specifically, the CNFs-like suspension, (ii) the inlet opening and (iii) the wire gauzes to prevent the solid particles and creatures to prevent the strike with the dialysis tubing. In this study, the selected $NH_4^+$ impurity has a diameter of 1.5 Å, allowing these ions to travel through the dialysis tubing with a 5 kDa molecular weight cutoff. In contrast, when the same ions come into contact with the CNFs adsorbent, they do not escape back into the (bag) tubing due to the concentration gradient and the binding of $NH_4^+$ on polymeric CNFs. Due to electrostatic interactions and a concentration gradient, $NH_4^+$ continues to bind with the CNFs adsorbent until the saturation point is reached. We collected the contaminated fish water from a small aquarium (Fig. S2 and Table S7 in SI) and tested the $NH_4^+$ concentration before and after the remediation test. Table S7 in SI demonstrates the concentration of

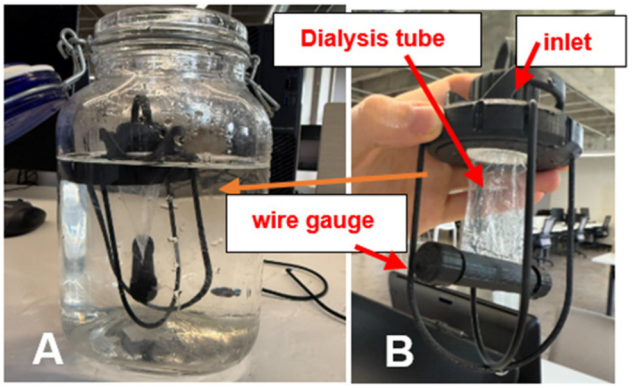


**Fig. 7** Demonstration of (A) FRS in contaminated water and (B) FRS design.

**Table 2** Comparative table depicting the $NH_4^+$ removal using different materials including CNFs

| Modification | Removal efficiency | Ref. |
|---|---|---|
| Cellulose nanofibers (CNFs) | 303 mg $g^{-1}$ | This study |
| Ultrasonically activated forestry waste biochar | 26.28 mg $g^{-1}$ | 17 |
| Ball-milled biochar | 22.9 mg $g^{-1}$ | 32 |
| Sulfonated reed waste biochar | 4.20–5.19 mg N $g^{-1}$ | 33 |
| MgO-biochar composite | 17.5 mg $g^{-1}$ | 34 |
| Straw biochar modified by soda residue | 3.87 mg $g^{-1}$ | 35 |
| Reverse osmosis cellulose acetate membranes | 98% | 36 |
| Bacterial cellulose activated carbon | 33.5–221.4 mg $g^{-1}$ | 18 |
| Nitro-oxidized cellulose nanofibers | 22.7 mg $g^{-1}$ | 27 |
| Cellulose sulfate nanofibers | 41.1 mg $g^{-1}$ | 19 |
| Crosslinked sulfonated polymer | 87% | 37 |
| MIEX resin | 98% | 38 |
| Pyridinium-type anion exchange resin | 94.3% | 39 |

$NH_4^+$ from the fish tank, before and after testing with the CNFs in the dialysis tube using the FRS. We have filled 0.1 g (0.5 wt% CNFs in 20 mL) into the dialysis tubing with a 5 kDa molecular weight cutoff and dipped it in the contaminated water collected from the fish tank. We have done three individual tests using the same stock of contaminated water. The results indicated that the system could absorb 80–90% $NH_4^+$ from real fish tank water. Fig. S1 in the SI presents the aquaponic system from which the contaminated water was collected. Our focus was on performing remediation of $NH_4^+$, so we measured the removal of $NH_4^+$ alone. The only problem we have noticed with this setup is the air gap that could be maintained in the tube while closing. The presence of this air gap allowed the water to move through the tubing along with $NH_4^+$, resulting in dilutions of CNFs in the tube. Still, we have observed a negligible change in the absorption capacity. This demonstrated that dialysis tubing can be an effective option for technically utilizing nanofibers or similar adsorbent materials, such as powders or nanoparticles, to capture impurities in water.

## Conclusions

In conclusion, this study provides a critical insight into the effectiveness of CNFs in adsorbing ammonium impurities from simulated and real contaminated water. CNFs with a negative surface charge, in the form of carboxylate groups, effectively removed ammonium impurities, achieving a maximum adsorption capacity of 303.3 mg $g^{-1}$. Additionally, the removal efficiency increased to 98% at a pH of 7, where the ammonium and ammonia both exist at equilibrium. The adsorption capacity of CNFs was evaluated under various conditions, including the amount of adsorbents, pH changes, time variations, and wastewater sources. The remediation experiment, conducted at an ammonium concentration of 500 ppm using a consistent amount of CNFs with 0.5 wt% under various conditions, provided more realistic results and demonstrated the versatility of CNFs in multiple situations. For example, 0.5 wt% of CNFs with 500 ppm ammonium, when mixed without pH alteration, showed a removal efficiency of 71.20%. In contrast, when the pH of the ammonium solution was altered, a 76.3% removal was observed at pH 5 with the same mixing conditions. The CNFs demonstrated the very high efficiency of 86.4–22.5% ammonium removal when tested against a range from 5 to 5000 ppm, respectively. CNFs are a layered structure with abundant negative surface charge, owing to ammonium removal *via* ion-exchange through the surficial functionality and multilayer adsorption through the layered structure. Therefore, the mechanism obeys both the Langmuir and the Freundlich isotherm models. In summary, CNFs are an eco-friendly, renewable, and sustainable material derived from abundant natural resources, offering tunable functionality and providing an attractive, scalable solution to various environmental remediation studies, with the added benefits of recycling and reusability as shown in this study.

## Author contributions

EMAA, SCH, MAM, SM, ARR, JJK, PS, and MK designed the experiments. EMAA, SCH, SM, MAM, and JJK acquired and analyzed the data. The manuscript was compiled, written, and revised by PS, JS, AKS, WB, and SM. All authors gave approval to the final version of the manuscript.

## Conflicts of interest

The authors declare that they have no conflict of interest.

## Data availability

Data will be made available upon request from the authors. The Supplementary Information file includes Histograms for Figures 3A, B, and C. Effect of pH on ammonium removal efficiency and adsorption. Effect of CNFs dose on ammonium removal efficiency and adsorption capacity. Adsorption efficiency and experimental parameters for $NH_4^+$ removal using CNFs. Relationship between the values of $Q_e$ and $C_e$. Effect of time on ammonium removal efficiency and adsorption capacity. Time-dependent adsorption and kinetic parameter values. The initial and final ammonium concentrations of real contaminated fish water tank samples using CNFs in the dilute bag of FRS for remediation. See DOI: https://doi.org/10.1039/d5lp00201j.

## Acknowledgements

P. R. S. would like to thank the Start-up grant (2023–2026) from the Western Michigan University Department of Chemical and Paper Engineering.

## References

1 V. Yadav, M. Rani, L. Kumar, N. Singh and V. Ezhilselvi, *Water, Air, Soil Pollut.*, 2022, **233**, 465.
2 K. G. Sellner, G. J. Doucette and G. J. Kirkpatrick, *J. Ind. Microbiol. Biotechnol.*, 2003, **30**, 383–406.
3 K. Tewari, *Phycology*, 2022, **2**, 244–253.
4 E. Zohdi and M. Abbaspour, *Int. J. Environ. Sci. Technol.*, 2019, **16**, 1789–1806.
5 D. W. Schindler, S. R. Carpenter, S. C. Chapra, R. E. Hecky and D. M. Orihel, *Environ. Sci. Technol.*, 2016, **50**, 8923–8929.
6 S. Sonak, K. Patil, P. Devi and L. D'Souza, *Environ. Pollut. Prot.*, 2018, **3**, 40–55.
7 D. M. Anderson, E. Fensin, C. J. Gobler, A. E. Hoeglund, K. A. Hubbard, D. M. Kulis, J. H. Landsberg, K. A. Lefebvre, P. Provoost and M. L. Richlen, *Harmful Algae*, 2021, **102**, 101975.

8 A. Omar, F. Almomani, H. Qiblawey and K. Rasool, *Sustainability*, 2024, **16**, 2112.
9 B. Thamdrup, *Annu. Rev. Ecol. Evol. Syst.*, 2012, **43**, 407–428.
10 P. Purwono, H. Hadiyanto and M. Budihardjo, *Int. J. Eng.*, 2023, **36**, 565–572.
11 G. Wastensson and K. Eriksson, *Crit. Rev. Toxicol.*, 2020, **50**, 219–271.
12 J. Berberich, T. Li and E. Sahle-Demessie, in *Separation science and technology*, Elsevier, 2019, vol. 11, pp. 285–328.
13 M. A. Abdelaziz, M. E. Owda, R. E. Abouzeid, O. Alaysuy and E. I. Mohamed, *Int. J. Biol. Macromol.*, 2023, **225**, 1462–1475.
14 Z. Karim, M. Hakalahti, T. Tammelin and A. P. Mathew, *RSC Adv.*, 2017, **7**, 5232–5241.
15 B. Han, C. Butterly, W. Zhang, J.-z. He and D. Chen, *J. Cleaner Prod.*, 2021, **283**, 124611.
16 Y. Wang, L. Chen, Y. Zhu, W. Fang, Y. Tan, Z. He and H. Liao, *Environ. Sci. Eur.*, 2024, **36**, 25.
17 T. Wang, G. Li, K. Yang, X. Zhang, K. Wang, J. Cai and J. Zheng, *Sci. Total Environ.*, 2021, **778**, 146295.
18 A. Khamkeaw, W. Sanprom and M. Phisalaphong, *Case Stud. Chem. Environ. Eng.*, 2023, **8**, 100499.
19 K. I. Johnson, W. Borges, P. R. Sharma, S. K. Sharma, H.-Y. Chang, M. M. Abou-Krisha, A. G. Alhamzani and B. S. Hsiao, *Nanomaterials*, 2024, **14**, 507.
20 P. R. Sharma, B. Zheng, S. K. Sharma, C. Zhan, R. Wang, S. R. Bhatia and B. S. Hsiao, *ACS Appl. Nano Mater.*, 2018, **1**, 3969–3980.
21 P. R. Sharma, A. Chattopadhyay, C. Zhan, S. K. Sharma, L. Geng and B. S. Hsiao, *Cellulose*, 2018, **25**, 1961–1973.
22 H. Chen, S. K. Sharma, P. R. Sharma, K. Chi, E. Fung, K. Aubrecht, N. Keroletswe, S. Chigome and B. S. Hsiao, *Cellulose*, 2021, **28**, 8611–8628.
23 P. R. Sharma, A. Chattopadhyay, S. K. Sharma, L. Geng, N. Amiralian, D. Martin and B. S. Hsiao, *ACS Sustainable Chem. Eng.*, 2018, **6**, 3279–3290.
24 P. R. Sharma, A. Chattopadhyay, S. K. Sharma and B. S. Hsiao, *Ind. Eng. Chem. Res.*, 2017, **56**, 13885–13893.
25 H. Chen, P. R. Sharma, S. K. Sharma, A. G. Alhamzani and B. S. Hsiao, *Nanomaterials*, 2022, **12**, 4156.
26 K. I. Johnson, *State University of New York at Stony Brook*, 2022.
27 K. I. Johnson, G. Ilacas, R. Das, H.-Y. Chang, P. R. Sharma, C. O. Dimkpa and B. S. Hsiao, *Sustainability Sci. Technol.*, 2024, **1**, 014001.
28 P. R. Sharma, X. Huang, M. Yang, S. K. Sharma and B. S. Hsiao, *Sustainable Separation Engineering: Materials, Techniques and Process Development*, 2022, pp. 563–589.
29 F. Bettaieb, M. A. Abdelaziz, I. S. Alatawi, M. A. Aljowni, H. Parveen, S. Mukhtar, N. Omer, R. Jame, S. A. Alshareef, M. E. Owda and Y. A. Bin Jardan, *Int. J. Biol. Macromol.*, 2025, **310**, 143354.
30 D. L. Sparks and D. L. Suarez, *Rates of Soil Chemical Processes*, Soil Science Society of America, Inc., 1991.
31 A. Al Mamun, Y. M. Ahmed, M. a. F. R. AlKhatib, A. T. Jameel and M. A. AlSaadi, *Nano*, 2015, **10**, 1550017.
32 Y. Qin, X. Zhu, Q. Su, A. Anumah, B. Gao, W. Lyu, X. Zhou, Y. Xing and B. Wang, *Environ. Geochem. Health*, 2020, **42**, 1579–1587.
33 M. Zhang, R. Sun, G. Song, L. Wu, H. Ye, L. Xu, S. J. Parikh, T. Nguyen, E. Khan and M. Vithanage, *Environ. Pollut.*, 2022, **292**, 118412.
34 R. Xiao, H. Zhang, Z. Tu, R. Li, S. Li, Z. Xu and Z. Zhang, *Environ. Sci. Pollut. Res.*, 2020, **27**, 7493–7503.
35 L. Liu and M. Zhang, *Int. J. Environ. Sci. Technol.*, 2023, **20**, 13783–13798.
36 A. Bódalo, J.-L. Gómez, E. Gómez, G. Leon and M. Tejera, *Desalination*, 2005, **184**, 149–155.
37 M. G. Torquato, E. C. Corrêa Torquato, A. C. L. Moraes, F. d. A. Buás Campeão, R. José França, M. R. d. C. Marques and L. d. C. Costa, *Macromol. Symp.*, 2022, **406**, 2200052.
38 Y. Yang, Z. Zheng, W. Ji, M. Yang, Q. Ding and X. Zhang, *Surf. Interfaces*, 2019, **17**, 100385.
39 L. Fu, J. Zu, H. Wang and X. Pan, *J. Radioanal. Nucl. Chem.*, 2019, **322**, 2043–2048.